

Electron-Transfer Chain Catalysis of η^2 -Arene, η^2 -Alkene, and η^2 -Ketone Exchange on Molybdenum

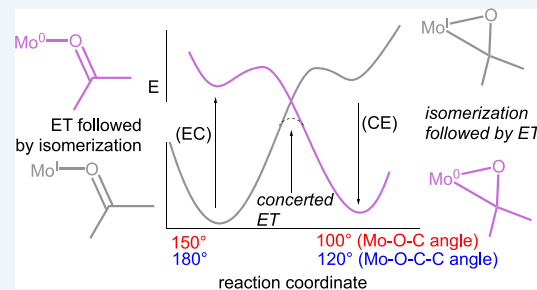
Steven J. Dakermanji, Jacob A. Smith, Karl S. Westendorff, Emmit K. Pert, Andrew D. Chung, Jeffery T. Myers, Kevin D. Welch, Diane A. Dickie,[✉] and W. Dean Harman[✉]

Department of Chemistry, University of Virginia, Charlottesville, Virginia 22904, United States

Supporting Information

ABSTRACT: An oxidant-initiated, substitution process for dihapto-coordinated ligands is described for the $\{\text{MoTp}(\text{NO})(\text{DMAP})\}$ system. Complexes of the form $\text{MoTp}(\text{NO})(\text{DMAP})(\eta^2\text{-alkene})$, $\text{MoTp}(\text{NO})(\text{DMAP})(\eta^2\text{-ketone})$, and $\text{MoTp}(\text{NO})(\text{DMAP})(\eta^2\text{-arene})$ (where Tp = hydridotris(pyrazolyl)borate and DMAP = 4-(dimethylamino)pyridine) undergo an alkene-to-ketone exchange that is catalyzed by the addition of <0.1 equiv of a metallocene oxidant (ferrocenium, permethylferrocenium, or cobaltocenium). A similar acceleration was observed in the presence of the H-bond donor hexafluoroisopropanol (HFIP). From experimental observations, a radical chain propagation mechanism is proposed that is dependent on the equilibrium between dihapto-coordinated ($\text{C}, \text{O}-\eta^2$) and monocoordinated ($\kappa\text{-O}$) isomers and the differing redox characteristics of these two isomeric forms. This concept was then applied to the search of sodium-free reduction conditions for the conversion of $\text{MoTp}(\text{NO})(\text{DMAP})(\text{I})$ to various molybdenum(0) complexes of unsaturated ligands, including $\text{MoTp}(\text{NO})(\text{DMAP})(\eta^2\text{-naphthalene})$ and $\text{MoTp}(\text{NO})(\text{DMAP})(\alpha\text{-pinene})$.

KEYWORDS: ETC-catalysis, molybdenum, acetone, pinene, redox-catalysis, dihapto



INTRODUCTION

Ligand substitution reactions play a fundamental role in organotransition-metal chemistry. Like their organic counterparts, they can proceed via either two-electron or one-electron mechanisms, and can be associative, dissociative, or concerted in nature.^{1,2} Which mechanism applies to a given reaction is dependent on the metal geometry, oxidation state, electron configuration, and nature of the ligand. Generally, octahedral d^6 complexes for second- and third-row transition-metal complexes have a tendency to undergo dissociative substitution, in which the departing ligand detaches prior to the incoming ligand binding to the metal (see Figure 1).¹ For these reactions, the specific rate of dissociation (k) has a tendency to strongly correlate with the metal–ligand bond dissociation free energy (BDFE), ΔG , which approaches the free energy of activation (ΔG^\ddagger).³ Such has been our experience with octahedral complexes of $\text{Os}(\text{II})$,⁴ $\text{Ru}(\text{II})$,^{5,6} $\text{Re}(\text{I})$,^{7,8} $\text{W}(0)$,^{8,9} and $\text{Mo}(0)$,^{8,10} where the outgoing ligand is a dihapto-coordinated alkene, arene, or carbonyl (e.g., ketone).

It is in this context that we set out to measure specific rates of substitution for various alkene and arene complexes of the molybdenum π -base $\{\text{MoTp}(\text{NO})(\text{DMAP})\}$. A plot of the M–L bond dissociation free energy (BDFE) vs ΔG^\ddagger for several arenes and α -pinene (Figure 2, top) shows a good correlation for complexes of the form $\text{MoTp}(\text{NO})(\text{DMAP})(\text{L})$ that undergo solvolysis in acetone, where L is an arene or alkene.

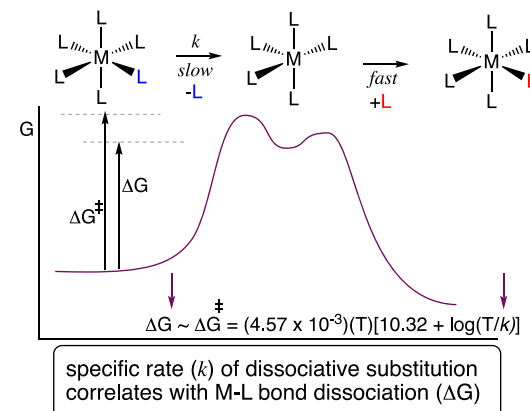
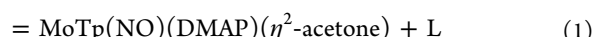


Figure 1. General mechanism for dissociative substitution and the relationship between the specific rate and M–L bond dissociation free energy (BDFE), ΔG .



For the four examples we measured, the calculated free energies were roughly 3–5 kcal/mol lower than the activation

Received: September 28, 2019

Revised: October 17, 2019

Published: October 21, 2019

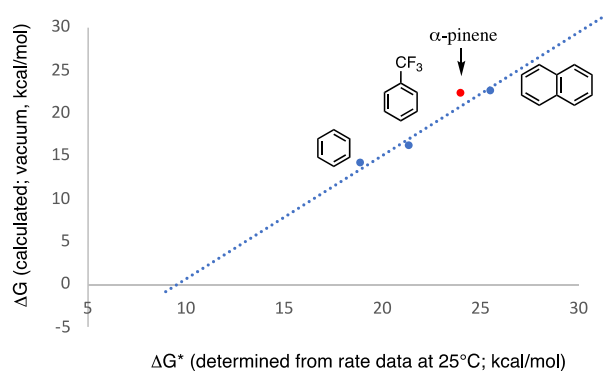


Figure 2. (Top) Relationship of experimentally determined activation free energies (ΔG^\ddagger) and calculated free energies (ΔG) of dissociation for $\text{MoTp}(\text{NO})(\text{DMAP})(\text{L})$. (Conditions: 25 °C, substitution in neat acetone.) (Bottom) Calculated free energies versus estimated substitution half-lives at 25 °C. Red areas indicate the binding locations.

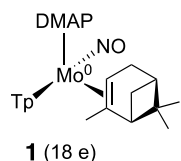
free energies in acetone (see Table 1), based on the application of the Eyring equation to the measured specific rates of

Table 1. Experimental Activation Free Energies (ΔG^\ddagger) and Calculated Free Energies (ΔG) of Dissociation (298 K) for $\text{MoTp}(\text{NO})(\text{DMAP})(\text{L})$

ligand	ΔG (DFT, kcal/mol)	ΔG^\ddagger (expt, kcal/mol)
THF	12.0	—
benzene	14.0	19.0
CF_3Ph	16.1	21.5
naphthalene	22.5	25.6
α -pinene	22.2	24.0
cyclohexene	25.9	—
pyridine	23.8	—
CO	43.4	—

substitution at 25 °C. Extrapolating this relationship to several other ligands (THF, cyclohexene, pyridine, and CO) led to estimates for substitution half-lives for these ligands (Figure 2, bottom), assuming that the dissociative substitution mechanism is still operative.

The α -pinene complex **1** has been shown to be a valuable synthon for $\{\text{MoTp}(\text{NO})(\text{DMAP})\}$ and was chosen for an in-depth study (where Tp^- is a 6e donor, NO^+ is a 2e donor, and DMAP and pinene are neutral 2e donors).¹¹



In order to prove that the above extrapolation was valid, we needed to prove that these substitution reactions were dissociative. Thus, for the ligand exchange reaction of **1**, we examined the rate dependence on the nature and concentration of the incoming ligand (see Table 2). Complex **1** was

Table 2. Kinetic Data for **1 (~10 mM) Reacting with Various Ligands**

ligand, L	cmpnd	NMR yield (%)	half-life deuterated solvent (h)	$\Delta G^\ddagger(25^\circ\text{C})$ (kcal/mol)
benzaldehyde (0.1 M benzene- d_6)	2	70	1.5	—
benzaldehyde (0.1 M benzene- d_6) with 0.1 equiv of FeCp_2^+	2	>90	<0.1	—
benzaldehyde (0.1 M benzene- d_6) passed through basic alumina with 0.5 equiv FeCp_2	2	40	17.5	23.9
benzaldehyde (0.1 M benzene- d_6) passed through basic alumina	2	46	14.8	—
acetone (neat)	3	89	10.3	23.9
acetone (neat) with 0.1 equiv FeCp_2^+	3	93	0.6	—
acetone (0.1 benzene- d_6)	3	88	16.3	24.2
acetone (neat) with 0.1 equiv FeCp_2^+ and 1.5 equiv Et_3N	3	91	1.1	—
acetone- d_6 (10% D_2O)	3	58	6.8	—
acetone- d_6 (10% D_2O) with 0.1 equiv CoCp_2^+	3	95	0.9	—
naphthalene (0.1 M benzene- d_6)	5	75	15.6	24.1
ethyl acetate (0.1 M benzene- d_6)	6	49	15.5	24.1
acetonitrile (neat)	7	58	11.5	24.0
DMF (neat)	8	63	15.0	24.1
pyridine (0.8 M in THF) ^a	16	—	26	24.4
PMMe_3 (0.8 M in THF) ^a	17	—	26	24.4

^aAs determined by cyclic voltammetry. FeCp_2^+ used as PF_6^- , BArF_6^- , or Tf_2N^- salt.

found to undergo clean replacement with a variety of other ligands ($\text{L} =$ naphthalene, ethyl acetate, acetonitrile, pyridine, PMMe_3) to form $\text{MoTp}(\text{NO})(\text{DMAP})(\text{L})$, with specific rates similar to those found for acetone.¹¹ In most cases, half-lives ranged from 10 h to 26 h at 25 °C ($\Delta G^\ddagger = 24.2 \pm 0.3$ kcal/mol), and were largely insensitive to the chemical nature and concentration of the incoming ligand (i.e., neat or as a benzene or THF solution). However, an outlier was revealed when we examined the displacement of the α -pinene ligand of **1** with benzaldehyde. Instead of a half-life of ~10 h to form $\text{MoTp}(\text{NO})(\text{DMAP})(\eta^2\text{-CO-benzaldehyde})$, **2**, displacement of the pinene occurred with a half-life of 1.5 h. Complexes of the form $\{\text{MoTp}(\text{NO})(\text{DMAP})(\text{L})\}$ are known to be susceptible to oxidation by Brønsted acids.^{12,13} The erratic behavior of the benzaldehyde reaction with pinene complex **1**

was thought to be the result of contamination of benzaldehyde with benzoic acid, which was speculated to be playing a catalytic role. Supporting this notion, when the aldehyde was first passed through basic alumina, the half-life for the conversion of **1** to **2** was increased to 14.8 h. Furthermore, when the reaction was repeated with 0.5 equiv of the mild *reductant* $[\text{Fe}(\text{Cp})_2]$ ($E_{1/2} = 0.55$ V, NHE in THF), the rate of ligand substitution was suppressed to the point that the half-life (17.5 h) approximated those of other ligands (see Table 2). This unusual feature was reminiscent of behavior exhibited by $[\text{Os}(\text{NH}_3)_5(\text{acetone})]^{2+}$, which was reported to undergo an acetone/acetone- d_6 exchange mechanism,¹⁴ that involved an adventitious *one-electron oxidant*.¹⁴ We suspected a similar electron transfer chain (ETC) catalysis mechanism¹⁵ was in play with the reaction of benzaldehyde and the α -pinene complex **1**. Alkene complexes of π -basic metal complexes can be highly substitution-inert, and establishing a process for ligand displacement under mild conditions could provide a valuable synthetic tool.

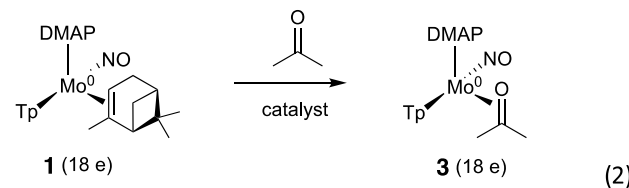
RESULTS AND DISCUSSION

Preliminary Observations. To test the theory that ligand substitution on $\{\text{MoTp}(\text{NO})(\text{DMAP})\}$ could be catalyzed by redox-active species, we repeated the reaction of α -pinene complex **1** and benzaldehyde, along with 0.5 equiv (1.6 mM) of the oxidant $[\text{Fe}(\text{Cp})_2](\text{Tf}_2\text{N})$ (where $\text{Tf}_2\text{N}^- = \text{bis}(\text{trifluoromethanesulfonyl})\text{imide}$). Ferrocenium salts are commonly used as redox catalysts in organic synthesis¹⁶ and organometallic chemistry.¹⁵ Under the influence of this ferrocenium additive, the exchange was complete within $\ll 6$ min, and the yield *improved* to 90%, as monitored by ^1H NMR spectroscopy (see Table 2). Similar to that seen with benzaldehyde, the displacement of pinene by acetone to form $\text{MoTp}(\text{NO})(\text{DMAP})(\eta^2\text{-acetone})$, **3**, could be catalyzed. In this case, 0.1 equiv of $[\text{Fe}(\text{Cp})_2](\text{Tf}_2\text{N})$ (1.0 mM) reduced the half-life from 10.3 h to 0.6 h.

Ferrocenium salts can act as Lewis acids.¹⁶ In order to rule out a mechanism involving this function of the ferrocenium additive, 1.5 equiv of Et_3N was added to a solution of the pinene complex in acetone, and permethylferrocenium (0.040 V vs NHE, $[\text{Fe}(\text{Cp}^*)_2]\text{PF}_6$) salt was used as the redox catalyst in place of $[\text{Fe}(\text{Cp})_2](\text{Tf}_2\text{N})$. Even in the presence of the amine additive, the weaker oxidant $[\text{Fe}(\text{Cp}^*)_2](\text{Tf}_2\text{N})$ still accelerated ligand exchange ($t_{1/2} = 1.1$ h) at a rate similar to that observed with ferrocenium ion ($t_{1/2} = 0.6$ h).

Since water is a common impurity in acetone,¹⁷ we also investigated its role in the substitution reaction. When the pinene complex **1** was dissolved in acetone- d_6 and monitored with 10% D_2O added, the yield was found to decrease from 89% to 58%. However, the rate of the reaction *increased*. This observation suggested that, like the benzoic acid impurity, the water may be reacting in such a way as to generate an adventitious redox-active species that could catalyze the ligand exchange. Remarkably, even when cobaltocenium ion (-0.78 V cf. 0.55 V (NHE) for $[\text{Fe}(\text{Cp})_2]^+$), a weaker oxidant compared to the iron salts, was present, along with 10% D_2O , displacement of pinene by acetone not only happened at an accelerated rate ($t_{1/2} = 0.9$ h), but the yield was increased from 58% to 95% (see Table 1). The water additive, which had drastically compromised the substitution reaction in acetone alone, seemingly had no effect once the cobalt salt was included.

Kinetics Analysis. To study the mechanism of this redox-catalyzed substitution more closely, the displacement of α -pinene by acetone was explored in greater depth (see eq 2):



Using ^1H NMR signals corresponding to an H4 proton of a pyrazolyl ring for **1** (6.10 ppm) and for **3** (6.15 ppm; Figure 3), kinetic data were obtained for the reaction shown in eq 2.

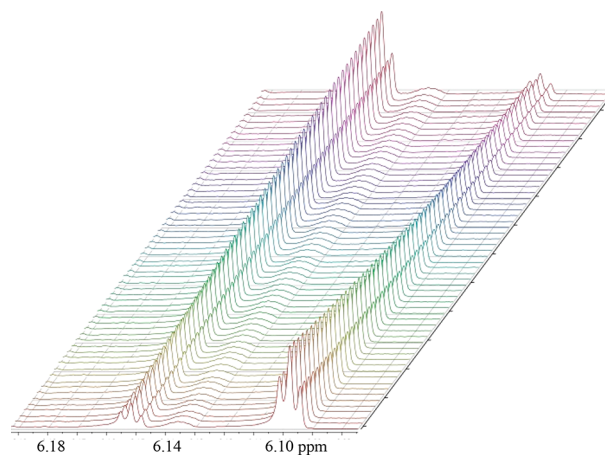


Figure 3. ^1H NMR data for the conversion of **1** to **3**. Initial conditions: $[\mathbf{1}] = 50$ mM; $[\text{Fe}(\text{Cp})_2](\text{BARF}) = 5$ mM.

As seen in Figure 3, the decrease of the pinene complex (6.10 ppm) is accompanied by the concomitant growth of the acetone complex (6.15 ppm). A plot of $\ln[\mathbf{1}]$ vs time was found to be linear (see Figure 4) for both the uncatalyzed

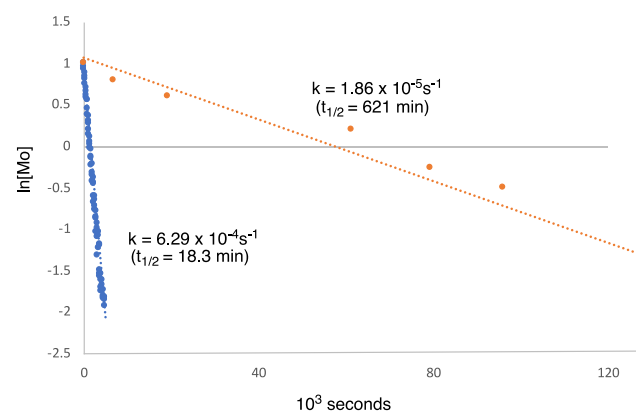


Figure 4. Comparison of catalyzed and uncatalyzed substitution reactions.

reaction and for the reaction with 0.1 equiv $[\text{Fe}(\text{Cp})_2](\text{BARF})$ added. These data indicate that (i) both reactions are operating under pseudo-first-order kinetics, and (ii) the addition of 0.1 equiv of the oxidant (5 mM) enhances the rate by more than 30-fold.

To test the relationship between the catalyst loading ($[O]^\circ$) and rate of the reaction (k_{obs}), multiple trials were conducted at different initial concentrations of the metallocene salt **O**. A standardized 17 mM solution of **1** was treated with a catalyst loading from $[O]^\circ = 0, 0.25, 0.5, 1.0, 2.5, 3.0$, and 4.0 mM, using ferrocenium, permethylferrocenium, and cobaltocenium cations as their tetrakis[3,5-bis(trifluoromethyl)phenyl]borate (BArF) salts. First-order rate constants (k_{obs}) were obtained, and the specific rate for the uncatalyzed reaction, k_{uncat} , was subtracted from k_{obs} to determine k_{cat} (i.e., when $[O]^\circ = 0$, $k_{uncat} = 1.86 \times 10^{-5} \text{ s}^{-1}$), where

$$k_{obs}[A] = k_{uncat}[A] + k_{cat}[A] \quad \text{and} \quad k_{obs} = k_{uncat} + k_{cat} \quad (3)$$

Data points were collected in triplicate for each concentration and averaged. Values obtained for k_{cat} were plotted versus $[O]^\circ$, as shown in Figure 5.

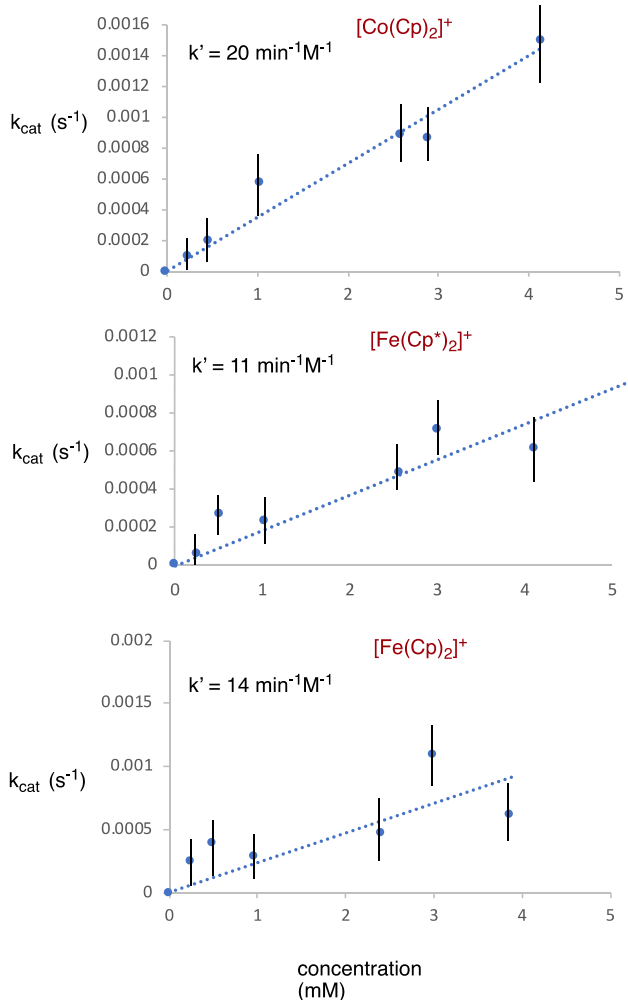


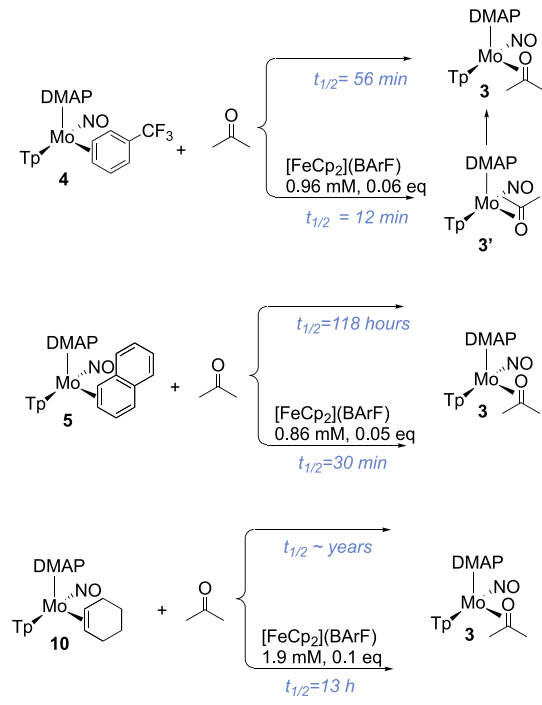
Figure 5. Plot of k_{cat} vs time, for the redox-catalyzed substitution of pinene for acetone.

Remarkably, while the rate of the reaction was determined to be dependent on the initial concentration of **O**, it was *largely independent of the O/R redox potential, despite differences in reduction potentials of over 1.3 V*. The slope ($k' = k_{cat}/[O]$) for ferrocenium ($k' = 14 \pm 5 \text{ min}^{-1} \text{ M}^{-1}$), permethylferrocenium ($k' = 11 \pm 5 \text{ min}^{-1} \text{ M}^{-1}$), and cobaltocenium ($k' = 20 \pm 5 \text{ min}^{-1} \text{ M}^{-1}$) were almost indistinguishable, within experimental

error. Significantly, for the case of cobaltocenium ion (2.9 mM), even though it was the weakest oxidant, the addition of 12 equiv of Et₃N had only a minor effect of the catalysis rate ($k_{cat} = 0.00063 \text{ s}^{-1}$ with NEt₃, compared to 0.00088 s^{-1} without NEt₃). In contrast, a similar amount of the nonbasic amide DMAc (8 equiv) more effectively inhibited the catalysis ($k_{cat} = 0.00039 \text{ s}^{-1}$ with DMAc, compared to 0.00088 s^{-1} without DMAc).

Similar to the behavior of the pinene-to-acetone exchange, whose half-life at 1 mM loading of Fe(Cp)₂⁺ was 38 min (Figure 5), the conversions of arene complexes MoTp(NO)-(DMA)^{-(η²-naphthalene)} and MoTp(NO)(DMA)^{-(η²-trifluorotoluene)} to acetone complex **3** were also catalyzed by the one-electron oxidants (see Scheme 1).

Scheme 1. Acceleration of Exchange Reactions with the Addition of Ferrocenium



For the trifluorotoluene complex (**4**, 16 mM), the reaction half-life is reduced from 56 min to 12 min at relatively low catalytic loading (0.06 equiv, 1.0 mM). In addition to the expected product **3**, an additional molybdenum complex was observed at early time points in the ¹H NMR spectra. This transient species, which was thought to be a second isomer of the acetone complex in which the carbonyl is oriented away from the DMAP ligand (Scheme 1), converted to the major isomer with an approximate half-life of 50 min under these conditions. For the naphthalene complex **5**, the addition of 0.05 equiv of Fe(Cp)₂BARF (0.86 mM) decreases the half-life from 118 h to 30 min. A plot of ln[S] vs time again shows linear behavior, indicating pseudo-first-order behavior (see Figure 6). We note here that, while the uncatalyzed substitution reactions for the trifluorotoluene complex (55 min), pinene complex (16 h), and naphthalene complex (~5 days) widely vary, the addition of ~1 mM of [Fe(Cp)₂]⁺ ($\ll 1$ equiv) results in substitution half-lives that are all on the order of minutes. For the cyclohexene complex **10**, substitution in acetone is undetectable after several days in solution ($t_{1/2}$ is

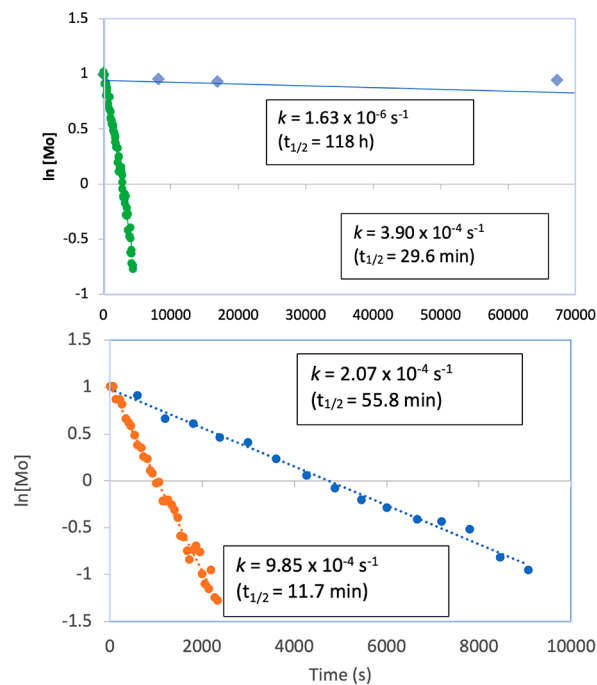


Figure 6. Catalyzed and uncatalyzed substitution reactions. (Bottom) TFT complex (**4**, 16 mM) with and without $[\text{Fe}(\text{Cp})_2](\text{BArF})$ (1.0 mM). (Top) Naphthalene complex (**5**, 17 mM) with and without $[\text{Fe}(\text{Cp})_2](\text{BArF})$ (~ 0.86 mM).

estimated to be ~ 30 years; see Figure 2), but in the presence of ~ 2 mM $[\text{Fe}(\text{Cp})_2]^+$, the half-life was determined to be ~ 13 h at 25°C .

While the previously described experiments of the catalytic substitution reaction on $\{\text{MoTp}(\text{NO})(\text{DMAP})\}$ focused primarily on acetone as the incoming ligand, other molecules with the potential to form π -complexes were also explored. Despite its bulky *t*-butyl group, pinacolone was also found to be suitable as the incoming ligand, and the displacement of α -pinene for this ketone showed significant acceleration in the presence of $[\text{Fe}(\text{Cp})_2](\text{BArF})$ (0.1 equiv, 2 mM). However, we note that the relative substitution rates for pinacolone were found to be slower than those observed for acetone. The displacement of pinene for *R*-camphor and *R*-fenchone also could be catalyzed, but like pinacolone, the acceleration of the reaction rate was more modest than for acetone at similar concentrations. Furthermore, the displacement reactions with these two terpenoid ketones were accompanied by significant decomposition. Other carbonyl-containing compounds such as ethyl acetate or DMF failed to show any increase in substitution rate upon exposure to $[\text{Fe}(\text{Cp})_2](\text{BArF})$ (0.1 equiv, 2 mM). In contrast, aldehydes such as benzaldehyde and *R*-myrtenal showed dramatic acceleration, significantly faster than that observed for acetone at low catalyst loading $[\text{Fe}(\text{Cp})_2](\text{BArF})$ (0.1 equiv, 2 mM). These results are summarized in Table 3.

Displacement of the pinene ligand in **1** with acetonitrile in the presence of the metallocene salts resulted in immediate decomposition, with no diamagnetic structures identifiable in ^1H NMR spectra after an hour. Attempts to catalyze the exchange of pinene (from **1**) for cyclohexene, trifluorotoluene, or naphthalene were also unsuccessful using metallocene salts.

Mechanism. Based on the above observations, an ETC catalysis cycle is proposed (see Scheme 2). The process is

Table 3. Half-Lives for Substitution in the Presence and Absence of $[\text{Fe}(\text{Cp})_2]^+$

L	Half-life (h)	Half-life (h) with $[\text{Fe}(\text{Cp})_2](\text{BArF})^a$	Cpd #
$\text{H} \text{---} \text{C}(=\text{O}) \text{---} \text{Ph}$	10	<0.1	2
$\text{H} \text{---} \text{C}(=\text{O})$	15	0.3	3
$\text{H} \text{---} \text{C}_6\text{H}_4 \text{---} \text{C}_6\text{H}_5$ THF solvent	15.6	15.6	5
$\text{H} \text{---} \text{C}(=\text{O}) \text{---} \text{OEt}$	15.5	15.5	6
$\text{H} \text{---} \text{C}(=\text{O}) \text{---} \text{NMe}_2$	15.0	15.0	8
$\text{H} \text{---} \text{C}(=\text{O}) \text{---} \text{C}_6\text{H}_4 \text{---} \text{C}_6\text{H}_5$	4	<0.1	9
$\text{C}_6\text{H}_5 \text{---} \text{C}_6\text{H}_4 \text{---} \text{C}_6\text{H}_5$ THF co-solvent	15	15	10
$\text{H} \text{---} \text{C}(=\text{O}) \text{---} \text{C}_6\text{H}_3(\text{CH}_3)_2$	19	10	11

^a $[\text{Fe}(\text{Cp})_2](\text{BArF}) \approx 2$ mM, 0.1 equiv (298 K).

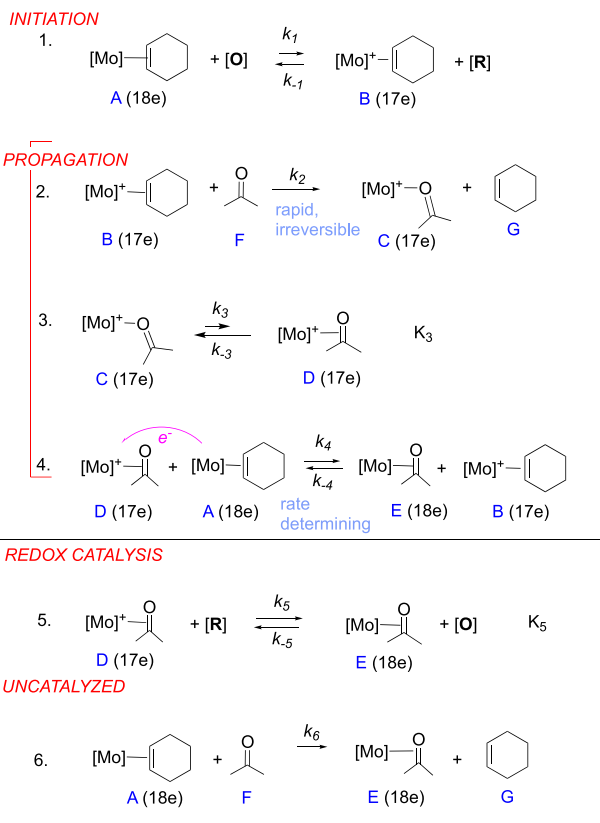
initiated by the metallocenium salt (**O**) oxidizing the alkene or arene complex (**A**). In its oxidized form, the resulting molybdenum(I) complex (**B**) undergoes rapid and irreversible ligand displacement to form the ketone complex **C**. This species, while most stable in its κ^1 form, has access to the dihapto-coordinated isomer (**D**). Judging from the osmium analogue $[\text{Os}(\text{NH}_3)_5(\eta^2\text{-acetone})]^{2+}$,¹⁸ the dihapto-coordinate form is a much stronger oxidant than the $\kappa\text{---O}$ complex, and is capable of reacting, either with the starting complex **A** (step 4 in Scheme 2), or with the reduced form of the redox initiator (**R**) (step 5 in Scheme 2; electrocatalysis) to form the product ketone **E**, along with regeneration of the oxidized alkene complex **B**. In the latter scenario, **O** functions as a true catalyst, rather than as an initiator.

While it is possible for both the chain-propagation (i.e., step 4 in Scheme 2) and redox catalysis (i.e., step 5 in Scheme 2) mechanisms to be operative,¹⁹ the apparent insensitivity of the system to the **O/R** reduction potential (vide supra) leads us to believe that the process is best approximated as a chain process (steps 1–4 in Scheme 2), where **O** serves the role as an oxidative initiator.²⁰ Considering a scenario where eq 5 is inactive (no redox catalysis) and eq 4 is rate-limiting and irreversible ($k_4[\text{B}][\text{E}] \approx 0$), then, after the initiation step,

$$\text{rate} = -\frac{d[\text{A}]}{dt} = k_4[\text{D}][\text{A}] = k_4[\text{C}]K_3[\text{A}] + k_6[\text{A}] \quad (4)$$

where K_3 describes the η^2/κ^1 equilibrium for the acetone linkage isomerization on Mo(I). Taking the concentration of acetone (solvent) as a constant, and assuming that step 2 in Scheme 2 is rapid and irreversible, all of **O** is immediately

Scheme 2. Mechanistic Steps for the ETC-Catalyzed Exchange of Alkene for a Ketone, Where Ketone Isomerization on Mo(I) Precedes Electron Transfer (a Chemical-Electrochemical (CE) Propagation)



converted to C, which is taken to be at a steady-state concentration for the course of the reaction:

$$[\mathbf{O}]^0 = [\mathbf{C}]$$

$$\frac{-d[\mathbf{A}]}{dt} = k_{\text{obs}}[\mathbf{A}] = K_3 k_4 [\mathbf{O}]^0 [\mathbf{A}] + k_6 [\mathbf{A}]$$

$$k_{\text{obs}} = (K_3 k_4 [\mathbf{O}]^0 + k_6) \quad (5)$$

Thus, from Figure 5,

$$k_{\text{obs}} - k_6 = k_{\text{cat}} = K_3 k_4 [\mathbf{O}]^0 = k' [\mathbf{O}]^0 \quad (6)$$

Under these conditions, a plot of k_{cat} vs $[\mathbf{O}]$ should be linear, and *independent* of the potential of \mathbf{O} , where the slope $k' = K_3 k_4$, but *independent* of the potential of the O/R half-reaction. Figure 5 shows this general behavior. Values for $k' = k_4 K_3$ range from $11 \text{ min}^{-1} \text{ M}^{-1}$ to $20 \pm 5 \text{ min}^{-1} \text{ M}^{-1}$, largely independent of the nature of the oxidant. Under this scenario, the following characteristics are explained:

- Where the concentration of incoming ligand \mathbf{F} is constant ($\sim 10 \text{ M}$), the reaction obeys first-order kinetics, and the half-life of the reaction is dependent on the concentration of \mathbf{O} .
- The rate of the reaction is largely independent of the reduction potential E° for \mathbf{O} over a range of $\sim 1.3 \text{ V}$. If \mathbf{O} was acting as a redox catalyst, with step 5 in Scheme 2 being rate-determining, then the reaction rate should be dependent exponentially on the O/R reduction potential. Presumably, the reason this catalysis works, even with $[\text{Co}(\text{Cp})_2]^+$, is that its conjugate $[\mathbf{R}] =$

$[\text{Co}(\text{Cp})_2]$ reacts with either acetone or water impurities and is thus removed from the system.²¹

- As the carbonyl changes from aldehyde to ketone, K_3 is expected to decrease as the equilibrium shifts toward the κ^1 isomer. Correspondingly, the observed rate of substitution is found to decrease as K_3 decreases. While it is possible that the amide (DMAc) substitution reactions are not thermodynamically favorable, an inhibitory effect was nonetheless observed, even in an acetone solvent.
- The more readily the alkene complex A is oxidized, the faster the reaction should be. This rate (k_4) should be dependent on the $\text{Mo}(\text{I})/\text{Mo}(\text{0})$ formal reduction potential (E°), but also on the rate of subsequent loss of ligand (k_2). These features are approximated through cyclic voltammetry: the more rapid k_2 , the more the $E_{\text{p},\text{a}}$ will shift negative, and the more rapid the redox-catalyzed substitution reaction is expected to be.²⁰ Because of their $E_{\text{r}}C_i$ nature, formal reduction potentials for the molybdenum alkene complexes are not easily determined, yet there is a clear correlation between the catalyzed specific rate of the substitution reaction (k_{obs}) and $E_{\text{p},\text{a}}$ (the anodic peak potential of the complex at 100 mV/s; see Figure 7): A faster off-rate is expected to both shift the anodic peak potential negative and minimize the back-reaction of step 4 in Scheme 2.

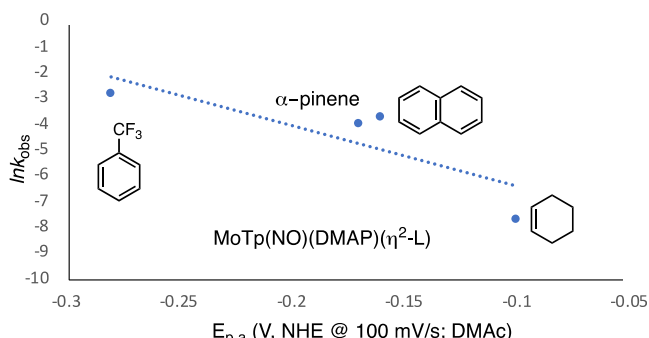


Figure 7. Plot of $\ln k_{\text{obs}}$ for substitution in acetone vs $E_{\text{p},\text{a}}$ of the molybdenum(0) alkene complex.

- Triethylamine does not significantly alter the catalysis, but the amide DMAc largely inhibits the reaction. Triethylamine can absorb protons (neutralizing any acid-catalysis pathway) but cannot easily bind to the molybdenum center. The amide, on the other hand, can form a κ^1 complex whose potential is far too negative (approximately -1200 mV , NHE) to be reduced in a reaction step analogous to step 4 in Scheme 2. In other words, K_3 is too small to be relevant, with κ^1 dominating over η^2 .

While the mechanism in Scheme 2 provides an explanation for many of the features of the alkene/ketone substitution reaction, an alternative mechanism in which electron transfer is followed by a change in ketone hapticity should also be considered. In this scenario (Scheme 3), the relevant ketone linkage isomerization involves molybdenum(0) rather than molybdenum(1). Thus, the following question arises: does electron transfer precede ketone isomerization (Scheme 3) or follow it (Scheme 2)? A cyclic voltammogram of the acetone complex 3 at 100 mV/s is particularly revealing (see Figure 8).

Scheme 3. Mechanistic Steps for the ETC-Catalyzed Exchange of Alkene for a Ketone, Where Ketone Isomerization on Mo(0) Follows Electron Transfer (an Electrochemical–Chemical (EC) Propagation)

INITIATION

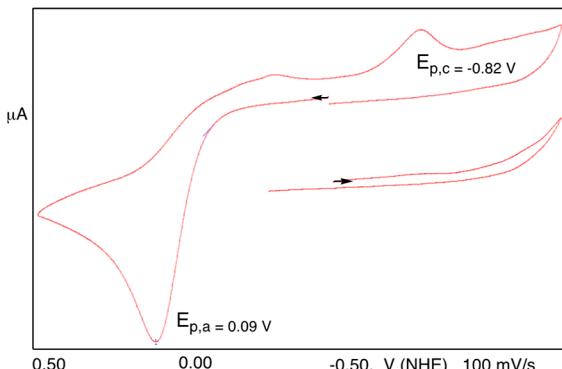
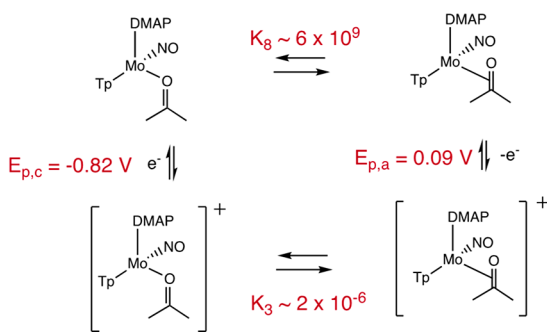
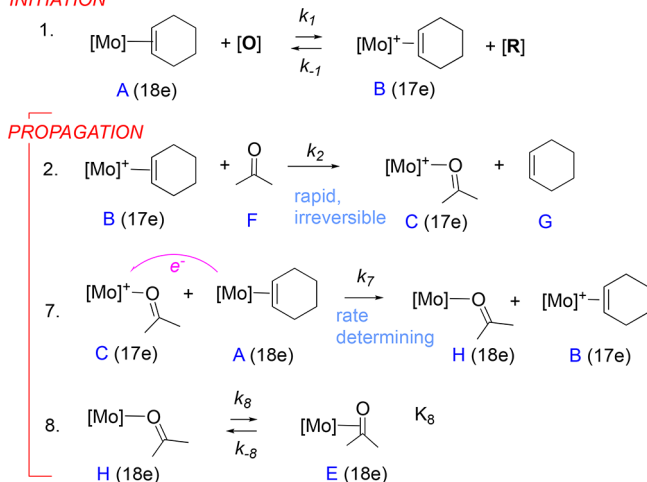


Figure 8. (Bottom) Cyclic voltammogram of acetone complex **3** in an acetone solvent; scan rate = 100 mV/s, TBAH electrolyte. (Top) ECEC electrochemical mechanism proposed for acetone complex **3**.

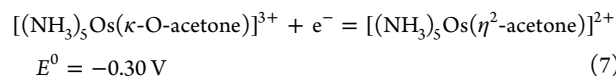
It shows a broad anodic wave with $E_{p,a}$ at 0.09 V (oxidation of $\text{Mo}(0)-\eta^2\text{-acetone}$) and a cathodic wave at $E_{p,c}$ at -0.82 V (reduction of $\text{Mo}(1)-\kappa\text{O-}\text{acetone}$). At faster scan rates, the anodic wave shifts positive and the cathodic wave shifts negative, consistent with an ECEC mechanism²² in which the $\text{Mo}(0)-\eta^2\text{-acetone}$ rapidly opens to $\kappa\text{-O}$ following oxidation and the latter species rapidly closes to $\eta^2\text{-C}_3\text{O}$ following reduction of $\text{Mo}(1)\text{-}\kappa\text{O}$. A free-energy calculation of the $\text{Mo}(0)$ acetone equilibrium (Table 4) leads to a value for K_8 , and by estimating $E_{1/2}$ for each redox half reaction as $E_{p,a}$ and $E_{p,c}$, a

thermodynamic cycle provides a rough estimate of K_3 (see Figure 8).

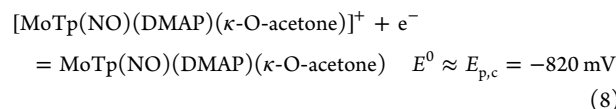
Table 4. Free Energies of Isomerization for Various Carbonyl Ligands on Molybdenum(0)

X, Y	ΔG isomerization (kcal/mol)	K_{eq} (298 K)	C–Mo bond length (Å)
H, H	-22.39	2×10^{16}	2.13
CH_3, CH_3	-13.38	6×10^9	2.18
$\text{CH}_3, \text{OCH}_3$	-7.88	6×10^5	2.21
$\text{CH}_3, \text{N}(\text{CH}_3)_2$	-0.46	2.2	2.27

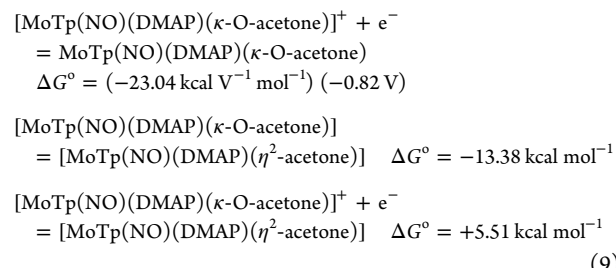
The electrochemical behavior of **3** in acetone (Figure 8) is similar to that of the pentaammineosmium(II) acetone complex, $[\text{Os}(\text{NH}_3)_5(\text{-}\eta^2\text{-acetone})](\text{OTf})_2$.²² Of note, the osmium complex was shown to be a much more potent reductant (-0.30 V) than its $E_{p,a}$ value ($+0.30 \text{ V}$) would indicate, because of the coupled linkage isomerization:



In a similar vein, the $\text{Mo}(\text{I})$ acetone complex (**C**) is likely to be an effective oxidant, because of the coupled $\kappa\text{-O}/\eta^2$ linkage isomerization on $\text{Mo}(0)$ (EC reaction; see Table 4). In order to get a sense of the oxidizing power of $[\text{MoTp}(\text{NO})(\text{DMAP})(\kappa\text{-O-acetone})]^+$ (**C**), one can estimate $E_{p,c}$ (-0.82 V) as being a rough approximation for the E^0 value for the $\kappa\text{-O-acetone}$ half-reaction:¹⁸



This half-reaction can be combined with the free energy calculated for the $\text{Mo}(0)$ equilibrium (see Table 4):



$$E^0 = \frac{-\Delta G^\circ}{nF} = \frac{-(5.51 \text{ kcal mol}^{-1})}{(1)(23.04 \text{ kcal V}^{-1} \text{ mol}^{-1})} = -0.24 \text{ V (NHE)} \quad (10)$$

According to eq 10, the $[\text{MoTp}(\text{NO})(\text{DMAP})(\kappa\text{-O-acetone})]^+$ species (**C**) is a capable oxidant with a potential (-0.24 V) similar to the $E_{p,a}$ value for $[\text{MoTp}(\text{NO})(\text{DMAP})(\eta^2\text{-alkene})]$ complexes (cf. cyclohexene complex (**10**), -0.10 V ; pinene complex (**1**), -0.170 V), when coupled with the ketone rearrangement. This reduction potential demonstrates the viability of steps 7 and 8 in Scheme 3.

Hence, electron transfer could occur prior to or after linkage isomerization. However, it may even be that the transition state for electron transfer involves a molybdenum–ketone geometry between those of the η^2 and κ -O isomers. As shown in Figure 9, both the Mo–O–C bond angle (88°–140°) and the Mo–

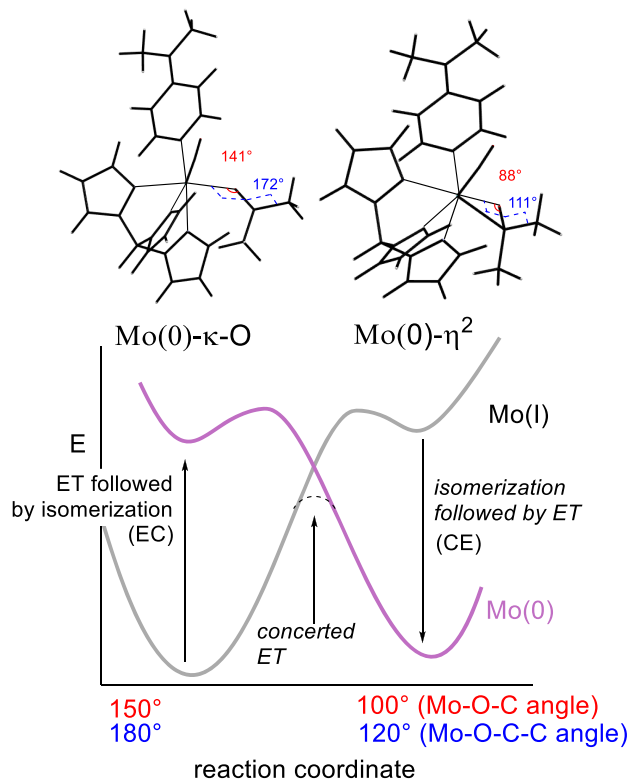


Figure 9. Proposed reaction coordinate for the Mo(I)-(κO-acetone) + e⁻ = Mo(0)-(η²-acetone) half reaction showing EC, CE, and concerted mechanisms. Bond and dihedral angles determined by density functional theory (DFT).

O–C–C dihedral angle (111°–172°) undergo significant changes as the Mo(0)–ketone complex changes from η^2 to κ -O. For these reasons, the ETC mechanism for alkene/acetone exchange is most conveniently considered to be concerted (step 9 in Scheme 4), where the sequence of isomerization and electron transfer (EC, CE, or concerted) does not need to be defined.

Using the model in Scheme 4, the rate of catalysis will still be dependent on the concentration of [O], but not its potential. Step 9 in Scheme 4 is rate-determining, with

$$\begin{aligned} -\frac{d[A]}{dt} &= k_9[C][A] + k_6[A] \quad \text{and} \quad [C](\text{steady-state}) \approx [O]^0 \\ -\frac{d[A]}{dt} &= k_9[O]^0[A] + k_6[A] \quad \text{and} \quad k_{\text{obs}} = (k_9[O] + k_6) \end{aligned} \quad (11)$$

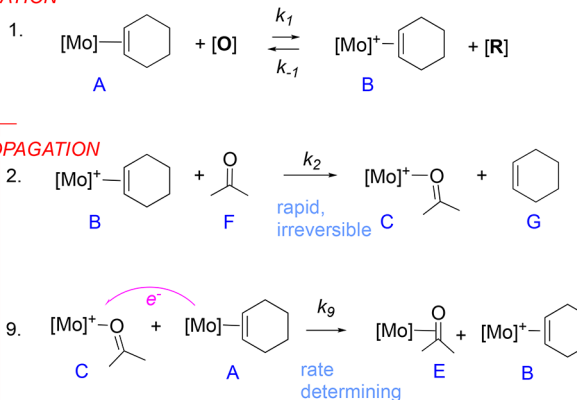
Thus,

$$k_{\text{obs}} - k_6 = k_{\text{cat}} = k_9[O]^0 \quad (= k'[O]^0) \quad (12)$$

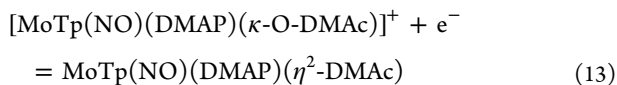
For this model, the same set of characteristics can be explained (vide supra, characteristics (a)–(e)) with the revision of characteristic (c): As the carbonyl changes from aldehyde to ketone to amide, K_8 , the ketone isomerization on Mo(0), decreases as the equilibrium shifts toward the κ^1 isomer. Correspondingly, the reduction potential for the half

Scheme 4. Concerted Electron-Transfer and Hapticity Change (Step 9) Incorporated into the ETC-Catalyzed Alkene/Ketone Ligand Exchange

INITIATION



reaction described in eqs 9 and 10 will decrease, which reduces the overall driving force (and rate) of the electron-transfer step. For example, for the amide DMAc, ΔG° is calculated to be +0.46 kcal mol⁻¹ and, therefore, for the half reaction



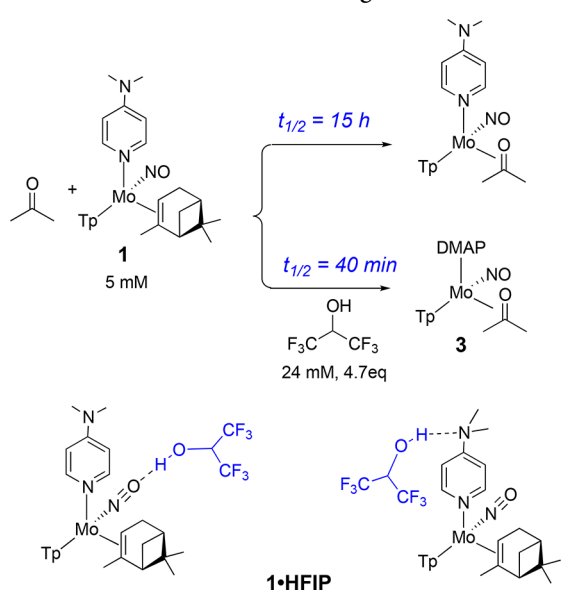
$E^\circ = -1.25$ V, making the overall potential for electron transfer (Step 9 in Scheme 4) unfavorable by ~1 V.

Acid Catalysis. In addition to the redox pathway outlined above, it was noted that the hydrogen donor hexafluoroisopropanol (HFIP) can also promote an acceleration of the ligand exchange reaction for MoTp(NO)(DMAP), albeit at much higher concentrations. In the case of the pinene complex 1, ligand exchange with acetone can be accelerated to rates similar to those observed with the metallocene salts. When the pinene complex 1 in an acetone solution is treated with ~25 mM (~5 equiv) of the strong H-donor HFIP, the half-life for substitution is reduced from 15 h to 40 min.

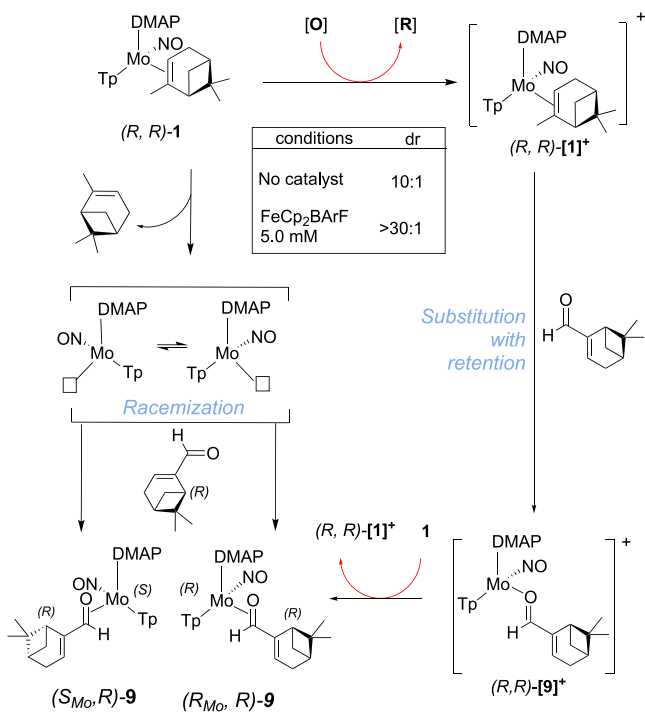
One scenario is that the HFIP forms a strong hydrogen bond with either the nitrosyl²³ or DMAP¹² ligand of 1, thereby reducing the electron density at the metal, and weakening the back-bonding interaction with the pinene ligand (see Scheme 5). However, upon further investigation, it was revealed that HFIP was undergoing an irreversible reaction with 1. A cyclic voltammogram of the reaction mixture containing 1 and HFIP in acetone shows values of $E_{\text{p,a}} = +250$ mV and $E_{1/2} = -1800$ mV, in addition to an anodic peak corresponding to the product acetone complex (3). These new features are similar to those found for MoTp(NO)(DMAP)(I), (15). Judging from CV and NMR data, the amount of desired product 3 is only ~10%–25%, and the remainder appears to be MoTp(NO)(DMAP)(κ^1 -OCH(CF₃)₂), as a result of alcohol oxidation of the molybdenum. Even with the bulkier fluorinated alcohol HOC(CF₃)₃, oxidation of the Mo(0) occurs. Together, these observations suggest that the accelerated ligand exchange may be a result of an adventitious oxidant generated from the reaction of molybdenum and the alcohol that initiates the chain propagation mechanism (vide supra), as opposed to an acid–base interaction.

Conservation of the Mo Stereogenic Center. Addition of a chiral ligand to the chiral molybdenum center forms diastereomers. This is illustrated in Scheme 6. In previous

Scheme 5. HFIP-Catalyzed Substitution of Pinene for Acetone via Either NO or DMAP Ligands



Scheme 6. Partial Racemization during Uncatalyzed Substitution



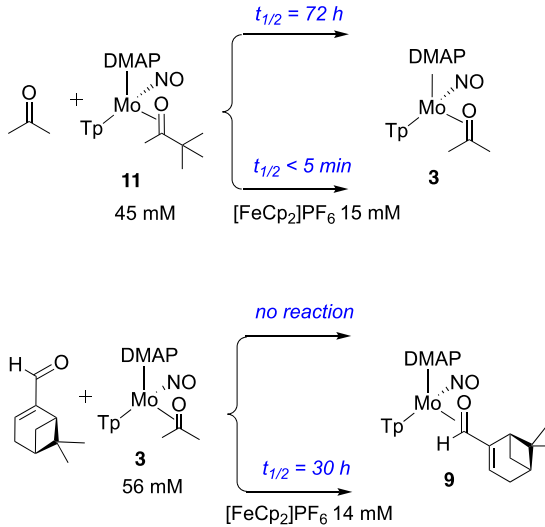
work, it was noted that, for the α -pinene complex (**1**), one of these diastereomers is unstable, and the complex is synthesized as a single diastereomer in which only one of the configurations of the molybdenum is present.¹¹ The synthesis of a single configuration of the metal complex is important, because it allows for synthesis of enantiopure organic products in subsequent chemical steps.^{11,24–26} However, in contrast to the rhenium and tungsten systems that we have studied,^{24–26} conversion from the molybdenum α -pinene complex **9** to a synthetically versatile aromatic ligand occurs with partial epimerization of the metal stereocenter.¹¹ Thus, the treatment of the pinene complex (*R, R*)-**1** with *R*-myrtenal produces a

10:1 mixture of two diastereomers. However, the addition of the ferrocenium ion not only catalyzed the ligand exchange reaction (**Scheme 6**), the myrtenal complex (**9**) diastereomer ratio was found to be increased to >30:1, demonstrating complete retention of the configuration of the metal stereocenter. As reported previously,¹¹ computational studies of the Mo(0) and Mo(I) square pyramidal intermediates indicate that the barrier to epimerization is ~3 kcal/mol higher for Mo(I); thus, the ligand displacement reaction via the higher oxidation state (e.g., (*R, R*)-[1]⁺) plays a key role in retention of the *R* configuration of the molybdenum. An additional reason for this enhancement may be the fact that 17e complexes can undergo substitution through an associative mechanism.^{1,2,20}

The conversion of the pinene complex **1** into the myrtenal complex **9** can also be accelerated by HFIP with full retention of the molybdenum stereocenter (>30:1), but, as described above, the HFIP is likely acting as a precursor to an uncharacterized oxidant, which initiates the ETC catalysis, in this case with stereochemical retention, but also with significant decomposition.

Ketone Displacement. As a general rule, η^2 -ketone complexes of {MoTp(NO)(DMAP)} are more stable than their η^2 -arene analogues. In order to exchange acetone with another ligand, high concentrations of an aldehyde were needed, and this reaction was only productive in the presence of a redox catalyst. The conversion of acetone complex **3** to myrtenal complex **9** is an example of such a reaction (**Scheme 7**): a myrtenal solution of **3** yields barely discernible quantities

Scheme 7. Examples of Redox-Catalyzed Ketone-to-Carbonyl Exchange

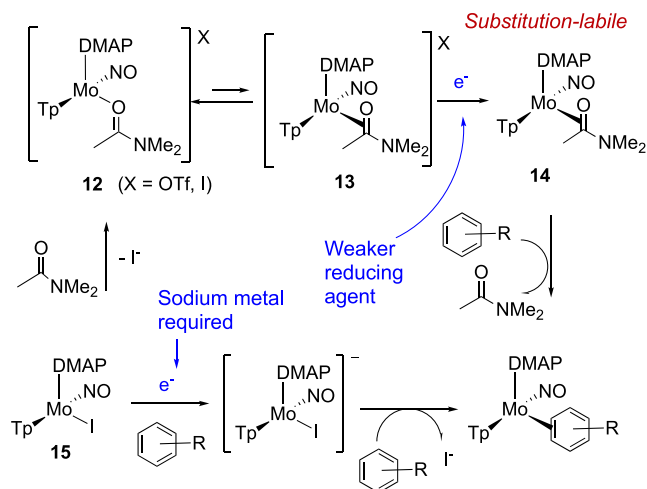


of the myrtenal complexes after 3 days. However, the addition of [Fe(Cp)₂]BArF (13.7 mM, 0.25 equiv) accelerates the reaction to the point that the half-life of the reaction is 30 h. A ketone with a large steric profile can also be exchanged for acetone. Thus, when the pinacolone complex **11** was subjected to redox catalyst (15 mM [Fe(Cp)₂]PF₆) in acetone, the half-life for this reaction can be cut from 72 h to <5 min (see **Scheme 7**).

As with arene and alkene exchanges with acetone, the studies described above rely on the ability of molybdenum complexes of aldehydes and ketones to exist as an κ^1/η^2 equilibrium of

isomers. We posited that it might be possible for a sufficiently sterically hindered or electron-rich carbonyl such as an amide to facilitate the reduction of the precursor $\text{MoTp}(\text{NO})(\text{DMAP})(\text{X})$ ($\text{X} = \text{OTf}$ or I) (**12** or **15**, respectively, in **Scheme 8**) to desirable $\text{Mo}(0)$ complexes. Our hope was that a

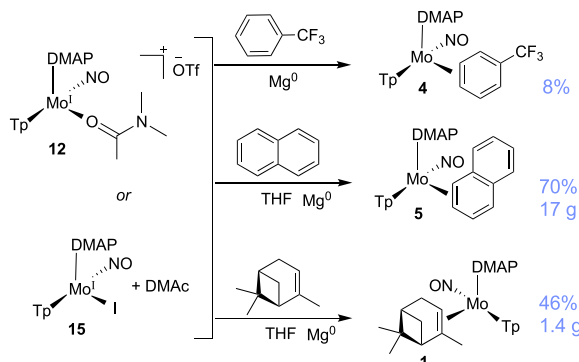
Scheme 8. Magnesium Reduction Pathway for the $[\text{Mo}-\text{DMAc}](\text{X})$ Salts ($\text{X} = \text{I}$ or OTf)



suitable ketone or amide $\text{Mo}(\text{I})$ complex (e.g., **12**) would have its $\text{Mo}(\text{I})/\text{Mo}(0)$ reduction coupled to a $\kappa\text{-O}$ to $\eta^2\text{-C},\text{O}$ isomerization (e.g., **13**), allowing the reduction to be performed using milder reducing agents than Na^0 metal.^{10,12} If the resulting $\text{Mo}(0)$ -carbonyl complex **14** was electronically or sterically destabilized, a second substitution reaction might be possible to form the desired $\text{Mo}(0)$ complex, according to **Scheme 8**.

Although the pinacolone complex **11** proved to be substitution-inert, it was known that $\text{Mo}(0)$ complexes could undergo ligand exchange in DMAc solvent without interference by the amide, so DMAc seemed like a good candidate for the process proposed in **Scheme 8**. Hence, the $\text{Mo}(\text{I})$ -DMAc complex was prepared from $\text{MoTp}(\text{NO})(\text{DMAP})(\text{CO})$ and silver triflate oxidant and isolated as the stable $\text{Mo}(\text{I})$ salt $[\text{MoTp}(\text{NO})(\text{DMAP})(\kappa\text{-DMAc})]\text{OTf}$ (**12**). A single crystal X-ray structure determination is described in the *Supporting Information*. This paramagnetic complex is characterized by an $\text{Mo}(\text{I}/0)$ reduction potential with $E_{1/2} = -1270$ mV. This reduction, which is likely coupled to the $\kappa\text{-O}$ - η^2 linkage isomerization, is ~ 200 mV more positive than the complexes $\text{MoTp}(\text{NO})(\text{DMAP})(\text{X})$ ($\text{X} = \text{Br}, \text{I}$) used as precursors to Mo η^2 -arene complexes.¹² This potential is right at the limit that untreated magnesium metal can normally access in non-aqueous solvents (approximately -1.3 V, ²⁷ NHE). Gratifyingly, magnesium powder, even without any pretreatment of the surface, was able to reduce the $\text{Mo}(\text{I})$ -DMAc complex to the corresponding $\text{Mo}(0)$ - η^2 -trifluorotoluene (**4**), naphthalene (**5**), and α -pinene products (see **Scheme 9**). As an example, the naphthalene complex **5** could be prepared on a 17 g scale in 70% overall yield from $\text{MoTp}(\text{NO})(\text{DMAP})(\text{I})$ (**15**), using pacified magnesium powder (untreated, 325 mesh), provided that DMAc (0.2% (v/v)) was included in the reaction mixture. Without the DMAc additive, only starting material was recovered after 1 week of monitoring. Compared to sodium reduction,¹² the magnesium reduction of **15** was completed within approximately the same time with 50% higher yield. In a

Scheme 9. Generation of $\text{Mo}(0)$ Arene and Alkene Complexes through Magnesium Powder (325 Mesh) Reduction



similar manner, the pinene (**1**, 46%) and TFT (**4**, 8%) complexes could be prepared, albeit with lower isolated yields. The ability to access compounds of the form $\text{TpMo}(\text{NO})(\text{DMAP})(\eta^2\text{- arene})$ without the need for pyrophoric metals constitutes a significant practical advance.

CONCLUSIONS

While electron transfer chain (ETC)-catalyzed substitution reactions have been well-documented,^{28,2,29} most of these studies have focused on κ^1 -bound ligands. This study demonstrates the role of this important mechanism for dihapto-coordinated aldehydes and ketones, particularly as the incoming ligand. These earlier studies on ETC substitution involve exchanging ligands that are similar in nature (e.g., one phosphine for another), and rarely involve removal of a carbonyl or alkene. Both CO and alkene ligands are considered to be strong π -acids and weak sigma donors. As a result, replacement with a better sigma donor (such as a phosphine, pyridine, or even THF) has a tendency to shift the 17e/18e reduction potential to much lower values. Hence, examples with this type of exchange are uncommon and have a tendency to be initiated by reduction to a 19 e intermediate, rather than initiated by oxidation.^{20,30,31} Similar to the earlier studies, exchange of alkenes by sigma donors on $\{\text{MoTp}(\text{NO})(\text{DMAP})\}$ cannot be catalyzed by oxidizing initiators. The critical role that ketones and aldehydes play as incoming ligands for ETC catalysis is their ability to dramatically change the reduction potential of the complex through a minimal geometrical change (κ to η^2). The large difference in reduction potentials brought about by the change in coordination mode provides the thermodynamic driving force required to propagate the ETC process.³²

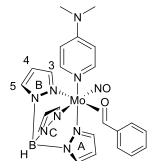
EXPERIMENTAL SECTION

General Methods. NMR spectra were obtained on 600 or 800 MHz spectrometers. All chemical shifts are reported in ppm, and proton and carbon shifts are referenced to tetramethylsilane (TMS), utilizing residual ^1H or ^{13}C signals of the deuterated solvents as an internal standard. Coupling constants (J) are reported in Hertz (Hz). Infrared spectra (IR) were recorded as a glaze on a spectrometer fitted with a horizontal attenuated total reflectance (HATR) accessory or on a diamond anvil ATR assembly. Electrochemical experiments were performed under a nitrogen atmosphere. Cyclic voltammetry data were taken at ambient temperature (~ 25 °C) at 100 mV/s in a standard three-electrode cell with a

glassy-carbon working electrode, *N,N*-dimethylacetamide (DMAc) or acetonitrile (CH₃CN) solvent (unless otherwise specified), and tetrabutylammonium hexafluorophosphate (TBAH) electrolyte (~0.5 M). All potentials are reported versus NHE (normal hydrogen electrode), using cobaltoenium hexafluorophosphate ($E_{1/2} = -0.78$ V), ferrocene ($E_{1/2} = +0.55$ V), or decamethylferrocene ($E_{1/2} = +0.04$ V) as an internal standard. The peak-to-peak separation was ~100–150 mV for all reversible couples. Unless otherwise noted, all synthetic reactions were performed in a glovebox under a dry nitrogen atmosphere. Deuterated solvents were used as received. Pyrazole (Pz) protons of the hydrido tris(pyrazolyl)-borate(Tp) ligand were uniquely assigned (e.g., “PzB3”), using a combination of two-dimensional NMR data. When unambiguous assignments were not possible, Tp protons were labeled as “Pz3/5” or “Pz4”. All J values for Pz protons are 2.0 ± 0.2 Hz. BH peaks (~4–5 ppm) are not identified, because of their quadrupole broadening; IR data are used to confirm the presence of a BH group (~2500 cm⁻¹). Compounds 1,¹¹ 3,⁸ 4,⁸ 5,³³ 6,¹¹ 7,¹¹ 8,^{11,34} and 9¹¹ have been previously reported.

All calculations were completed at the M06 level of theory, utilizing a hybrid basis set that used the LANL2DZ basis set for metal atoms and 6-31G(d,p) for all other atoms. Disassociation reaction energies were calculated without solvent effects, while isomerization energies were calculated in THF via an SMD model.

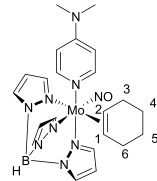
MoTp(NO)(DMAP)(η²-Benzaldehyde) (2).



A 4-dram vial was charged with a stir pea, MoTp(NO)-(DMAP)(η²-α,α,α-trifluorotoluene) (1.1 g, 1.7 mmol), and benzaldehyde (10 g, 98 mmol). This homogeneous light green mixture was capped and stirred for 10 min. This reaction mixture was then loaded onto a 60 mL coarse-porosity fritted disk that was two-thirds filled with silica gel. This column was washed with diethyl ether (50 mL) and a green band was isolated using THF (100 mL). The green solution was evaporated in vacuo to 20 mL and added to chilled pentane (100 mL), yielding a white precipitate that was collected on a 15 mL fine-porosity fritted disk. Some product had oiled out on the bottom of the filter flask, and this was dissolved in a minimal amount of DCM (~3 mL) and then added to ~50 mL of stirring chilled pentane. A white precipitate was isolated on a 15 mL fine-porosity fritted disk washed with chilled pentane (2 × 10 mL), and dried under static vacuum for 2 h, yielding 2 (0.52 g, 0.91 mmol, ~50% yield). IR: $\nu_{\text{NO}} = 1580$ cm⁻¹, $\nu_{\text{BH}} = 2484$ cm⁻¹. CV (THF; 100 mV/s): $E_{\text{pa}} = +0.40$ V. ¹H NMR (d^6 -acetone, δ): 7.95 (1H, d, Pz3/5), 7.92 (1H, d, Pz3/5), 7.88 (1H, d, Pz3), 7.78 (2H, m, DMAP H2 and H6), 7.56 (1H, d, Pz3/5), 7.48 (1H, d, Pz3/5), 7.32 (1H, d, Pz3), 7.28 (2H, t, $J = 7.84$, H3 and H5), 7.19 (2H, d, $J = 7.31$, H2 and H6), 7.02 (1H, t of t, $J = 7.25, 1.25$, H4), 6.65 (2H, m, DMAP H3 and H5), 6.29 (1H, t, Pz4), 6.24 (1H, t, Pz4), 6.23 (1H, t, Pz4), 4.45 (1H, s, aldehyde H), 3.10 (6H, s, DMAP methyls). ¹³C NMR (d^6 -acetone, δ): 155.7 (DMAP 4), 151.63 (DMAP 2 and 6), 149.13 (C1), 143.5 (Pz3/5), 143.5 (Pz3/5), 141.9 (Pz3/5), 136.8 (Pz3/5), 136.6 (Pz3/5), 136.3 (Pz3/5), 127.7 (C3 and C5), 126.30 (C2 and C6), 125.4 (C4), 107.6

(DMAP 3 and 5), 106.8 (Pz4), 106.3 (Pz4), 106.0 (Pz4), 98.1 (aldehyde carbonyl C), 39.2 (DMAP methyls). Calculated for C₂₃H₂₆BMoN₉O₂: C, 48.70; H, 4.62; N, 22.22. Found: C, 48.32; H, 4.63; N, 20.23. Calculated for 4(C₂₃H₂₆BMoN₉O₂)·CH₂Cl₂: C, 48.26; H, 4.93; N, 20.89.

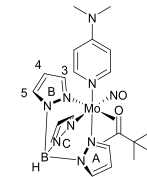
MoTp(NO)(DMAP)(η²-Cyclohexene) (10).



A 250 mL round-bottom flask was charged with a stir pea, sodium dispersion in paraffin wax (3 g, ~35% Na⁰ by weight, ~1.1 g Na⁰, 0.049 mol), and 250 mL of hexanes. The mixture was capped and allowed to mix vigorously for 18 h. The hexanes were then decanted and the remaining Na⁰ was crushed with a spatula to yield smaller grains. The sodium was then combined with ~100 mL of THF, cyclopentene (3.0 g, 0.037 mol), and then MoTp(NO)(DMAP)(1) (3.0 g, 0.0051 mol). The flask was recapped and allowed to mix 40 min. At this time, 100 mL of ether was added to the dark solution and the solution was allowed to mix for 30 s. The solution was then added to a 150 mL medium-porosity fritted disk approximately three-fourths filled with silica, and an orange band was eluted with 500 mL of ether. The orange ether solution was then concentrated in vacuo to dryness. The dried solid was dissolved in ~10 mL of DCM and then added to 200 mL of stirring hexanes. The orange solid was collected on a 30 mL fine-porosity fritted disk and washed with hexanes (3 × 25 mL). Desiccating for 2 h yielded an orange solid (1.4 g, 2.1 mmol, 42% yield). IR: $\nu_{\text{NO}} = 1547$ cm⁻¹, $\nu_{\text{BH}} = 2479$ cm⁻¹; CV: $E_{\text{pa}} = -0.10$ V, ¹H NMR (d^6 -acetone, δ): 8.05 (3H, s, DMAP 2 and 6 and PzA3), 7.88 (1H, d, PzC5), 7.85 (1H, d, PzAS), 7.77 (1H, d, PzB5), 7.56 (1H, d, PzC3), 7.20 (1H, d, PzB3), 6.65 (2H, m, DMAP 3 and 5), 6.30 (1H, t, PzC4), 6.28 (1H, t, PzA4), 6.11 (1H, t, PzB4), 3.06 (6H, s, DMAP methyl), 2.74 (1H, m, C3), 2.43 (2H, m, C3 and C6), 2.25 (1H, m, C2), 2.18 (2H, m, C1 and C6), 1.77 (2H, m, C4 and C5), 1.47 (1H, bm, C5), 1.37 (1H, bm, C4). ¹³C NMR (201 MHz, acetone) δ : 154.8 (DMAP 4), 150.9 (DMAP 2 and 6), 142.8 (TpA3), 141.9 (TpB3 or TpC3), 141.3 (TpA5 or TpC5), 137.2 (TpA5), 136.8 (TpB5), 135.6 (TpC5), 108.4 (DMAP 3 and 5), 106.4 (TpA4), 106.1 (TpB4 or TpC4), 106.1 (TpB4 or TpC4), 69.9 (C2), 63.6 (C1), 39.1 (DMAP methyl), 29.0 (C6), 28.7 (C3), 25.6 (C5), 24.5 (C5).

(Crystal structures are reported in the Supporting Information.)

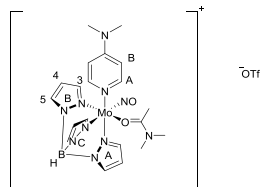
MoTp(NO)(DMAP)(η²-Pinacolone) (11).



A 4-dram vial was charged with a stir pea, MoTp(NO)-(DMAP)(η²-trifluorotoluene) (0.15 g, 0.00025 mol), and pinacolone (2.0 mL, 0.015 mol), and the solution was allowed to stir overnight (18 h). The off-white precipitate was then collected on a 15 mL fine-porosity fritted disk and washed with hexanes (3 × 10 mL). The solid was desiccated for 2 h under vacuum and collected (0.0729 g, 50%, ~5% paramagnetic

material impurities, as determined by CV). IR: $\nu_{\text{NO}} = 1554 \text{ cm}^{-1}$, $\nu_{\text{BH}} = 2514 \text{ cm}^{-1}$. CV (100 mV/s; NHE): $E_{\text{pa}} = +0.28 \text{ V}$ (broad). ^1H NMR (d_6 -acetone, δ): 8.25 (1H, d, PzA3), 7.90 (1H, d, PzB5), 7.87 (1H, d, PzC5), 7.83 (1H, d, PzA5), 7.62 (1H, d, PzB3), 7.54 (1H, d, PzC3), 7.46 (2H, m, DMAP H2 and H6), 6.51 (2H, m, DMAP H3 and H5), 6.28 (1H, t, PzA4), 6.27 (1H, t, PzB4), 6.17 (1H, t, PzC4), 3.06 (6H, s, DMAP methyls), 1.33 (9H, s, H 4), 1.01 (3H, s, H1). ^{13}C NMR (d_6 -acetone, δ): 155.5 (DMAP 4), 151.6 (DMAP 2 and 6), 147.1 (PzA3), 143.8 (PzC3), 143.2 (PzB3), 137.2 (PzA5), 136.1 (PzC5), 135.7 (PzB5), 110.9 (C2), 107.2 (DMAP 3 and 5), 106.6 (PzA4), 105.9 (PzB4), 105.8 (PzC4), 43.2 (C3), 39.2 (DMAP methyls), 30.5 (3C, C4 methyls), 22.6 (C1).

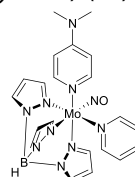
(MoTp(NO)(DMAP)(κ^1 -N,N-Dimethylacetamide))(OTf) (12).



A 50-mL round-bottom flask was charged with a small stir pea, MoTp(NO)(DMAP)(CO) (5 g, 10.2 mmol), and 25 mL DMA. Once the solution was stirring, AgOTf solid (2.6 g, 10 mmol) was added. [Caution: CO is released during the reaction.] Once bubbling had ceased, the solution was pulled through a 30 mL medium-porosity fritted disk, with a 1 cm layer of Celite to remove the solid. The Celite pad was washed with acetone until the green color was washed away ($\sim 5 \text{ mL}$). The DMA solution was then added to 600 mL of ether. The ether solution was decanted from the oily solid that was affixed to the sides of the precipitation flask. The gummy solid was dissolved in 50 mL of DCM and then transferred to a 150 mL medium-porosity fritted disk. The green solution was then allowed to drip into 1 L of stirring hexanes in a 2 L flask over the course of an hour. The precipitate in the hexane solution was then collected on a 150 mL medium-porosity fritted disk and washed with hexanes ($3 \times 100 \text{ mL}$), ether ($2 \times 100 \text{ mL}$), and then desiccated for 2 h. A mint green solid was collected (5.2 g, 7.4 mmol, 75% yield). IR: $\nu_{\text{NO}} = 1589 \text{ cm}^{-1}$, $\nu_{\text{BH}} = 2512 \text{ cm}^{-1}$. CV: $E_{\text{pa}} = 0.80 \text{ V}$, $E_{1/2} = -1.27 \text{ V}$. Anal. Calcd for $\text{C}_{21}\text{H}_{29}\text{BF}_3\text{MoN}_{10}\text{O}_5\text{S}$: C, 36.17; H, 4.19; F, 8.17; N, 20.09. Found: C, 35.97; H, 4.29; F, 7.91; N, 20.08.

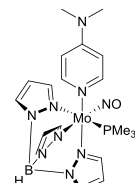
[MoTp(NO)(DMAP)(κ^1 -O-DMA)]OTf (Alternative Synthesis). To a 50 mL RBF charged with a small stir egg, MoTp(NO)(DMAP)(CO) (5 g, 10 mmol) was combined with 15 mL DMA. Once the solution was stirring, $\text{Cu}(\text{OTf})_2$ (1.85 g, 5.1 mmol) was added. [Caution: CO is released during the reaction.] Once bubbling had ceased, the solution was pulled through a 150 mL medium-porosity fritted disk, with a 1 cm layer of Celite to remove the silver solid. The Celite pad was washed with DMA until the green color was washed away ($\sim 5 \text{ mL}$). The DMA solution was added to 500 mL of ether and the green solid was collected on a 150 mL medium-porosity fritted disk and washed with ether ($3 \times 100 \text{ mL}$). The solid was desiccated and the green product was collected (4.7 g, 6.8 mmol, 67% yield). (0.061 g, 0.085 mmol, $\sim 50\%$ yield). IR: $\nu_{\text{NO}} = 1589 \text{ cm}^{-1}$, $\nu_{\text{BH}} = 2516 \text{ cm}^{-1}$. CV: $E_{\text{pa}} = 0.80 \text{ V}$, $E_{1/2} = -1.27 \text{ V}$.

Half-Life Determination for the Conversion of 1 to MoTp(NO)(DMAP)(η^2 -Pyridine) (16).



In a 4-dram vial with a stir pea, MoTp(NO)(DMAP)(η^2 - α -pinene) (0.29 g, 0.48 mmol), pyridine (0.31 g, 3.8 mmol), and THF (5 mL) were combined. This dark, homogeneous mixture was allowed to mix for $\sim 26 \text{ h}$. Approximately every 6 h, the reaction solution was monitored by CV. At 26 h, the reaction mixture appeared to be a 1:1 ratio of the MoTp(NO)(DMAP)(η^2 - α -pinene) starting material and MoTp(NO)(DMAP)(η^2 -pyridine) CV: $E_{1/2} = -0.92 \text{ V}$. The analogous compound WTp(NO)(PMe₃)(pyridine) has a value of $E_{1/2} = -0.78 \text{ V}$.³⁵ This compound was not isolated.

Half-Life Determination for the Conversion of 1 to MoTp(NO)(DMAP)(η^2 -PMe₃) (17).



In a 4-dram vial with a stir pea, MoTp(NO)(DMAP)(η^2 - α -pinene) (0.29 g, 0.48 mmol), pyridine (0.30 g, 3.9 mmol), and THF (5 mL) were combined. This dark, homogeneous mixture was allowed to mix for 26 h. Approximately every 6 h, the reaction solution was monitored by CV. At 26 h, the reaction mixture appeared to be a 1:1 ratio of the MoTp(NO)(DMAP)(η^2 - α -pinene) starting material and MoTp(NO)(DMAP)(PMe₃) ($E_{\text{pa}} = -0.17 \text{ V}$, compared to $E_{1/2} = -0.82 \text{ V}$). CV: $E_{1/2} = -0.82 \text{ V}$. The compound WTp(NO)(PMe₃)₂ has a value of $E_{1/2} = -0.61 \text{ V}$.³⁶ This compound was not isolated.

ASSOCIATED CONTENT

S Supporting Information

The Supporting Information is available free of charge on the ACS Publications website at DOI: 10.1021/acscatal.9b04191.

3-D Molecular structure of Mo κ -CO complex (MOL)

3-D Molecular structure of Mo κ -pyridine complex (MOL)

^1H NMR and ^{13}C NMR spectra, infrared spectra, cyclic voltammetric data, and X-ray data for selected compounds (PDF)

3-D Molecular structure of Mo κ -THF complex (MOL)

3-D Molecular structure of Mo benzaldehyde complex (MOL)

3-D Molecular structure of Mo benzaldehyde complex (MOL)

3-D Molecular structure of Mo benzaldehyde complex (MOL)

3-D Molecular structure of Mo κ -O-acetone complex (MOL)

3-D Molecular structure of Mo κ -O-acetone complex (MOL)

3-D Molecular structure of Mo κ -O-acetone complex (MOL)

3-D Molecular structure of Mo κ -O-acetone complex (MOL)
CIF files for compound 10 (CIF)
3-D Molecular structure of Mo benzaldehyde complex (MOL)

AUTHOR INFORMATION

Corresponding Author

*E-mail: wdh5z@virginia.edu.

ORCID

Diane A. Dickie: [0000-0003-0939-3309](https://orcid.org/0000-0003-0939-3309)

W. Dean Harman: [0000-0003-0939-6980](https://orcid.org/0000-0003-0939-6980)

Notes

The authors declare no competing financial interest.

ACKNOWLEDGMENTS

Acknowledgement is made to the National Science Foundation (No. CHE-1800051) for supporting this work.

REFERENCES

- (1) Astruc, D., Ligand Substitution Reactions. In *Organometallic Chemistry and Catalysis*; Astruc, D., Ed.; Springer: Berlin, Heidelberg, Germany, 2007; pp 121–134.
- (2) Howell, J. A. S.; Burkinshaw, P. M. Ligand Substitution Reactions at Low-valent Four-, Five-, and Six-coordinate Transition Metal Centers. *Chem. Rev.* **1983**, *83*, 557–599.
- (3) Bengali, A. A.; Leicht, A. Kinetic and Mechanistic Study of the Displacement of η^2 -Coordinated Arenes from $\text{Cp}^*\text{Re}(\text{CO})_2(\eta^2\text{C}_6\text{H}_5\text{R})$ ($\text{R} = \text{H}, \text{CH}_3, \text{C}(\text{CH}_3)_3$): Evidence for a Dissociative Mechanism and Estimation of the $\text{Re}-(\eta^2\text{-Arene})$ Bond Strength. *Organometallics* **2001**, *20*, 1345–1349.
- (4) Harman, W. D.; Sekine, M.; Taube, H. Substituent effects on η^2 -Coordinated Arene Complexes of Pentaammineosmium(II). *J. Am. Chem. Soc.* **1988**, *110* (17), 5725–5731.
- (5) Taube, H. Substitution Reactions of Ruthenium Ammines. *Comments Inorg. Chem.* **1981**, *1*, 17–31.
- (6) Isied, S. S.; Taube, H. Rates of Substitution in Cis and Trans Ruthenium(II) Aquotetraammines. *Inorg. Chem.* **1976**, *15*, 3070–3075.
- (7) Meiere, S. H.; Brooks, B. C.; Gunnoe, T. B.; Sabat, M.; Harman, W. D. A Promising New Dearomatization Agent: Crystal Structure, Synthesis, and Exchange Reactions of the Versatile Complex $\text{TpRe}(\text{CO})(1\text{-methylimidazole})(\eta^2\text{-benzene})$ (Tp = Hydridotris(pyrazolyl)borate). *Organometallics* **2001**, *20*, 1038–1040.
- (8) Myers, J. T.; Smith, J. A.; Dakermanji, S. J.; Wilde, J. H.; Wilson, K. B.; Shivokevich, P. J.; Harman, W. D. Molybdenum(0) Dihapto-Coordination of Benzene and Trifluorotoluene: The Stabilizing and Chemo-Directing Influence of a CF_3 Group. *J. Am. Chem. Soc.* **2017**, *139*, 11392–11400.
- (9) Graham, P. M.; Meiere, S. H.; Sabat, M.; Harman, W. D. Dearomatization of Benzene, Deamidization of N,N-Dimethylformamide, and a Versatile New Tungsten π Base. *Organometallics* **2003**, *22*, 4364–4366.
- (10) Mocella, C. J.; Delafuente, D. A.; Keane, J. M.; Warner, G. R.; Friedman, L. A.; Sabat, M.; Harman, W. D. Coordination Chemistry and Properties of Unusually π -Basic Molybdenum Fragments. *Organometallics* **2004**, *23*, 3772–3779.
- (11) Shivokevich, P. J.; Myers, J. T.; Smith, J. A.; Pienkos, J. A.; Dakermanji, S. J.; Pert, E. K.; Welch, K. D.; Trindle, C. O.; Harman, W. D. Enantioenriched Molybdenum Dearomatization: Dissociative Substitution with Configurational Stability. *Organometallics* **2018**, *37*, 4446–4456.
- (12) Myers, J. T.; Dakermanji, S. J.; Chastanet, T. R.; Shivokevich, P. J.; Strausberg, L. J.; Sabat, M.; Myers, W. H.; Harman, W. D. 4-(Dimethylamino)pyridine (DMAP) as an Acid-Modulated Donor Ligand for PAH Dearomatization. *Organometallics* **2017**, *36*, 543–555.
- (13) Myers, J. T.; Shivokevich, P. J.; Pienkos, J. A.; Sabat, M.; Myers, W. H.; Harman, W. D. Synthesis of 2-Substituted 1,2-Dihydronaphthalenes and 1,2-Dihydroanthracenes Using a Recyclable Molybdenum Dearomatization Agent. *Organometallics* **2015**, *34*, 3648–3657.
- (14) Harman, W. D.; Sekine, M.; Taube, H. Redox Promoted Linkage Isomerizations of Aldehydes and Ketones on Pentaammineosmium. *J. Am. Chem. Soc.* **1988**, *110*, 2439–2445.
- (15) Astruc, D. Electron-Transfer Chain Catalysis in Organotransition Metal Chemistry. *Angew. Chem., Int. Ed. Engl.* **1988**, *27*, 643–660.
- (16) Toma, Š.; Šebesta, R. Applications of Ferrocenium Salts in Organic Synthesis. *Synthesis* **2015**, *47*, 1683–1695.
- (17) Burfield, D. R.; Smithers, R. H. Desiccant Efficiency in Solvent Drying. 3. Dipolar Aprotic Solvents. *J. Org. Chem.* **1978**, *43*, 3966–3968.
- (18) Harman, W. D.; Sekine, M.; Taube, H. Redox-promoted Linkage Isomerizations of Aldehydes and Ketones on Pentaammineosmium. *J. Am. Chem. Soc.* **1988**, *110*, 2439–2445.
- (19) Hershberger, J. W.; Klingler, R. J.; Kochi, J. K. Kinetics, Thermodynamics, and Mechanism of the Radical-Chain Process for Ligand Substitution of Metal Carbonyls. *J. Am. Chem. Soc.* **1983**, *105*, 61–73.
- (20) Astruc, D. *Electron Transfer and Radical Processes in Transition-Metal Chemistry*; John Wiley & Sons: New York, 1995.
- (21) Watts, W. E. The Organic Chemistry of Metal-coordinated Cyclopentadienyl and Arene Ligands. In *Comprehensive Organometallic Chemistry*, Wilkinson, G.; Stone, F. G. A.; Abel, E. W., Eds.; Pergamon Press: Oxford, U.K., 1982; pp 1013–1071.
- (22) Harman, W. D.; Fairlie, D. P.; Taube, H. Synthesis, Characterization, and Reactivity of the $(\text{eta.}2\text{-acetone})$ -pentaammineosmium(II) complex. *J. Am. Chem. Soc.* **1986**, *108*, 8223–8227.
- (23) Sharp, W. B.; Legzdins, P.; Patrick, B. O. O-Protonation of a Terminal Nitrosyl Group To Form an η^1 -Hydroxylimido Ligand. *J. Am. Chem. Soc.* **2001**, *123*, 8143–8144.
- (24) Graham, P. M.; Delafuente, D. A.; Liu, W.; Myers, W. H.; Sabat, M.; Harman, W. D. Facile Diels-Alder Reactions with Pyridines Promoted by Tungsten. *J. Am. Chem. Soc.* **2005**, *127*, 10568–10572.
- (25) Wilson, K. B.; Myers, J. T.; Nedzbala, H. S.; Combee, L. A.; Sabat, M.; Harman, W. D. Sequential Tandem Addition to a Tungsten–Trifluorotoluene Complex: A Versatile Method for the Preparation of Highly Functionalized Trifluoromethylated Cyclohexenes. *J. Am. Chem. Soc.* **2017**, *139*, 11401–11412.
- (26) Ding, F.; Valahovic, M. T.; Keane, J. M.; Anstey, M. R.; Sabat, M.; Trindle, C. O.; Harman, W. D. Diastereo- and Enantioselective Dearomatization of Rhenium-Bound Naphthalenes. *J. Org. Chem.* **2004**, *69*, 2257–2267.
- (27) Lossius, L. P.; Emmenegger, F. Plating of magnesium from organic solvents. *Electrochim. Acta* **1996**, *41*, 445–447.
- (28) Hershberger, J. W.; Klingler, R. J.; Kochi, J. K. Electron-Transfer Catalysis. Radical Chain Mechanism for the Ligand Substitution of Metal Carbonyls. *J. Am. Chem. Soc.* **1982**, *104*, 3034–3043.
- (29) Geiger, W. E. Organometallic Electrochemistry: Origins, Development, and Future. *Organometallics* **2007**, *26*, 5738–5765.
- (30) Bezems, G. J.; Rieger, P. H.; Visco, S. Electron-induced nucleophilic substitution reactions in organometallic systems. *J. Chem. Soc., Chem. Commun.* **1981**, 265–266.
- (31) Karpinski, Z. J.; Kochi, J. K. Electron-transfer chain catalysis in the electrochemical deligation of bis(arene)iron(II) dication. Application of pulse voltammetric techniques as a mechanistic tool. *Inorg. Chem.* **1992**, *31*, 2762–2767.
- (32) Astruc, D. Transition-metal radicals: Chameleon Structure and Catalytic Function. *Acc. Chem. Res.* **1991**, *24*, 36–42.
- (33) Ha, Y.; Dilks, S.; Graham, P. M.; Liu, W.; Reichart, T.; Sabat, M.; Keane, J. M.; Harman, W. D. Development of Group 6 Dearomatization Agents. *Organometallics* **2006**, *25*, 5184–5187.

(34) Graham, P. M.; Mocella, C. J.; Sabat, M.; Harman, W. D. Dihapto-Coordinated Amide, Ester, and Aldehyde Complexes and Their Role in Decarbonylation. *Organometallics* **2005**, *24*, 911–919.

(35) Delafuente, D. A.; Kosturko, G. W.; Graham, P. M.; Harman, W. H.; Myers, W. H.; Surendranath, Y.; Klet, R. C.; Welch, K. D.; Trindle, C. O.; Sabat, M.; Harman, W. D. Isomerization Dynamics and Control of the η^2 /N Equilibrium for Pyridine Complexes. *J. Am. Chem. Soc.* **2007**, *129*, 406–416.

(36) Welch, K. D.; Harrison, D. P.; Lis, E. C.; Liu, W.; Salomon, R. J.; Harman, W. D.; Myers, W. H. Large-Scale Syntheses of Several Synthons to the Dearomatization Agent {TpW(NO)(PMe₃)} and Convenient Spectroscopic Tools for Product Analysis. *Organometallics* **2007**, *26*, 2791–2794.